Application of a Smoke Point Soot-Radiation Model in LES of Turbulent, Wall-bounded Diffusion Flames

Chatterjee P.*, Meredith K.V., Wang Y.

FM Global, Research Division, Norwood, MA 02062, USA.
**Corresponding author's email: prateep.chatterjee@fmglobal.com*

ABSTRACT

Buoyant, turbulent diffusion flames anchored on a slot burner in the presence of an isothermal wall have been numerically simulated. A laminar smoke point based subgrid (flamelet) radiation model has been applied toward estimation of overall radiant fractions and radiant power distributions of the ethylene fires. The model uses a turbulent micro-scale strain rate that influences the flamelet soot radiation. In the presence of the isothermal wall, the radiant fractions of the fires are observed to decrease along with a reduction of their peak radiant power output. Predicted radiant fractions and radiant power distributions are found to be reasonably close to the experimental data with improvements observed when the local strain rate is more accurately modeled as the maximum value between the numerical mesh-resolved and the micro-scale strain rates.

KEYWORDS: Buoyant flame, smoke point, soot radiation, wall cooling.

NOMENCLATURE

a_0	Micro-scale strain rate (s^{-1})	s	Stoichiometric oxygen to fuel ratio (-)
$a_{0,enh}$	Maximum of micro-scale and resolved strain rates (s^{-1})	$\tilde{S}_{ij}$	LES resolved strain rate tensor (s^{-1})
		T	Temperature (K)
$a_{\varepsilon,i}$	Emissivity weighting factors (-)	V_f	Flamelet volume (m^3)
A_f	Flamelet area (m^2)	$\tilde{Y}_F$	LES resolved fuel mass fraction (-)
$b_{\varepsilon,i,j}$	Emissivity polynomial coefficients (-)	$\tilde{Y}_{O_2}$	LES resolved oxygen mass fraction (-)
c_ε	Dissipation rate coefficient (-)	$\tilde{Z}$	LES resolved mixture fraction (-)
c_k	Turbulent viscosity coefficient (-)	**Greek**	
C	Eddy dissipation model coefficient (-)	Δ	LES filter size (m)
C_η	Strain rate coefficient (-)	ε	Emissivity (-)
f_v	Soot volume fraction (-)	ε_{sgs}	Subgrid turbulent dissipation rate (m^2/s^3)
$\tilde{h}^0$	LES resolved chemical enthalpy (J/kg)	κ_g	Gas-phase absorption coefficient (m^{-1})
$h^0_{F,\infty}$	Fuel heat of formation (J/kg)	κ_i	Gray gas absorption coefficient (m^{-1})
$\tilde{h}_s$	LES resolved sensible enthalpy (J/kg)	κ_s	Soot absorption coefficient (m^{-1})
H_p	Prior radiant/convective heat loss (-)	ν	Kinematic viscosity (m^2/s)
ΔH_c	Fuel heat of combustion (J/kg)	ν_t	Turbulent viscosity (m^2/s)
k_{sgs}	Subgrid turbulent kinetic energy (m^2/s^2)	$\bar{\rho}$	Density (kg/m^3)

Proceedings of the Ninth International Seminar on Fire and Explosion Hazards (ISFEH9), pp. 77-88
Edited by Snegirev A., Liu N.A., Tamanini F., Bradley D., Molkov V., and Chaumeix N.
Published by St. Petersburg Polytechnic University Press
ISBN: 978-5-7422-6496-5 DOI: 10.18720/spbpu/2/k19-46

ℓ_f	Mean turbulent flame height (m)	σ	Stefan-Boltzmann constant (W/m^2-K^4)
ℓ_m	Flamelet mean beam length (m)	τ_η	Turbulent micro time-scale (s)
p	Sum of partial pressures (Pa)	τ_m	LES mixing time-scale (s)
$\dot{q}_r'''$	Flamelet volumetric emission (W/m^3)	Ψ_r	Flamelet radiant emission fraction (-)
$\tilde{q}_r'''$	LES volumetric radiant emission (W/m^3)	$\tilde{\omega}_F'''$	LES fuel consumption rate (kg/m^3-s)

INTRODUCTION

Thermal radiation, dominated by radiative emission from soot, is primarily responsible for large-scale fire spread over solid combustible surfaces. Accurate estimations of spatio-temporal variations of radiant emission from the turbulent flame sheet is therefore important in large eddy simulations (LES) of fire growth. Flame radiant emission near solid surfaces is affected by the heat loss to these surfaces. The change in local turbulent micro-scale strain rate (defined in Refs. [1, 2]) can also be impacted by the presence of the surfaces, in turn affecting the flame-sheet radiant emission. In the present study, the effect of wall-induced cooling on buoyant flame characteristics is studied by considering inert walls, excluding other important phenomena like pyrolysis and fuel blowing normally occurring in wall-fire scenarios [1].

Soot-radiation from unconfined turbulent fires has previously been numerically simulated [1, 2] using an LES code, FireFOAM [1, 2]. In this study, the previously developed laminar smoke point [1] based subgrid soot-radiation model [1] has been applied toward predictions of radiant fractions and vertical distributions of radiant power of buoyant flames adjacent to an isothermal wall. The present study extends the slot burner investigation from Ref. [1] with the inclusion of a 2.2 m tall isothermal wall enclosure placed adjacent to the burner. In the authors' knowledge, this work is among the first to evaluate the near-wall performance of a turbulent soot-radiation model and compare the predicted results with experimental data. The aim of the study was to confirm the model formulation includes key physics required in modeling flame-sheet emission near walls. The study was conducted to establish the validity of the model in a complex configuration (wall-bounded flames) relevant to fire spread problems as compared to only modeling an unconfined diffusion flame.

NUMERICAL MODEL

LES of ethylene fires was conducted using a finite-volume solution technique with the application of subgrid models for turbulence and soot radiation [1, 2, 4]. The study focuses on the experimental setup of slot burner fires attached to an isothermal wall from the investigation of Markstein and de Ris [1].

LES TURBULENCE AND COMBUSTION MODELS

The LES code used was FireFOAM [4], which is based on the open source toolbox OpenFOAM [1]. The code solves fully compressible, three-dimensional reacting Navier-Stokes equations using the finite volume technique on unstructured meshes. Conservative forms of continuity, momentum, sensible enthalpy and species equations are solved with the PIMPLE (Pressure Implicit with Splitting of Operator) algorithm [8] applied for pressure-velocity coupling. The eddy dissipation model (EDM) [1] is used for combustion modeling. The EDM fuel consumption rate, $\tilde{\omega}_F'''$, is computed as

$$\tilde{\omega}_F''' = C\left(\overline{\rho}/\tau_m\right)\min\left(\tilde{Y}_F, \tilde{Y}_{O_2}/s\right), \quad (1)$$

where, $\overline{\rho}$ is the local density, the proportionality constant is $C = 4$, $\tilde{Y}_F$ and $\tilde{Y}_{O_2}$ are the filtered mass fractions of fuel and oxygen, respectively, and s is the stoichiometric oxygen to fuel ratio. The turbulent mixing-time is estimated as $\tau_m = k_{sgs}/\varepsilon_{sgs}$, where k_{sgs} and ε_{sgs} are the subgrid-scale (SGS) kinetic energy and its dissipation rate, respectively. In LES a substantial fraction of kinetic energy remains in the subgrid and in buoyant flows associated with fires the subgrid kinetic energy is evidently anisotropic in character. Therefore, transport of the subgrid kinetic energy is included for turbulence closure. The SGS turbulent viscosity, $\nu_t = c_k \Delta k_{sgs}^{1/2}$, in the momentum equations is computed from the solution of k_{sgs} as described in Fureby et al. [1]. The dissipation of k_{sgs} is modeled as $\varepsilon_{sgs} = c_\varepsilon k_{sgs}^{3/2}/\Delta$. The constant c_ε is equal to 1.048 and Δ is the LES filter size [10]. The turbulent viscosity is estimated from a localized dynamic procedure following the application of a test filter [1, 2]. The localized dynamic procedure produces a distribution of c_k to capture the dynamics of flow near the wall and in the laminar to turbulence transition region.

SUBGRID RADIATION MODEL

The present study uses a subgrid radiation model involving a two-dimensional laminar flamelet with fuel in the middle and oxidizer surrounding the fuel from two sides (see Fig. 1) [1, 2]. This is a representation of a fuel eddy in a turbulent flame being strained due to the presence of the local flow gradients. The turbulent flame-sheet is assumed to consist of an ensemble of such eddies. The model postulates a transient packet of fuel being stretched by a constant turbulent micro-scale strain rate normal to its axis [1]. The model applies the laminar smoke-point concept [6] to describe soot formation, oxidation and radiation. The effect of fuel type on soot radiation is modeled by assuming that the peak soot formation rate is inversely proportional to the fuel's laminar smoke point height [6]. Detailed description of the model formulation is available in Ref. [1]. The laminar smoke point height for ethylene (= 0.106 m) has been taken from Lautenberger et al. [6].

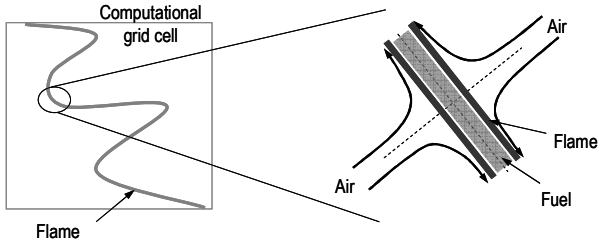

Fig. 1. Two-dimensional representation of the turbulent flame-sheet modeled as an ensemble of eddies.

The laminar flamelet equations

In the flamelet model, thermal radiation is assumed to be optically-thin and to occur primarily due to soot and gas-phase species (CO_2 and H_2O). The soot absorption coefficient is computed following Tien et al. [1] as

$$\kappa_s = 1226 f_v T \quad (\mathrm{m}^{-1}), \quad (2)$$

where T is the local flame temperature (K) and f_v is the soot volume fraction. The gas-phase absorption coefficient is estimated using the weighted sum of gray gases (WSGG) model [1] as

$$\kappa_g = -\ln(1-\varepsilon)/\ell_m \ , \tag{3}$$

where, ε is total emissivity over a mean beam length ℓ_m. The mean beam length is evaluated as [1]

$$\ell_m = 3.6 V_f / A_f \ , \tag{4}$$

where, V_f and A_f are flamelet volume and area, respectively, computed by assuming the entire flamelet is of a conical shape following the formulation in Ref. [16]. The mean beam length, ℓ_m, is computed to be ~4 mm. The emissivity is computed as

$$\varepsilon = \sum_{i=0}^{I} a_{\varepsilon,i}(T)\left(1 - e^{-\kappa_i p \ell_m}\right), \tag{5}$$

where $a_{\varepsilon,i}$ and κ_i are the emissivity weighting factor and absorption coefficient for the *i*-th fictitious gas, respectively, and p is the sum of partial pressures of all absorbing gases (CO_2 and H_2O). Following Smith et al. [2], in the present work three fictitious gray gases are used, and their temperature dependent emissivity weighting factors are computed as

$$a_{\varepsilon,i} = \sum_{j=1}^{J} b_{\varepsilon,i,j} T^{j-1}. \tag{6}$$

Here, $b_{\varepsilon,i,j}$ are the emissivity gas temperature polynomial coefficients, as defined in Ref. [17]. The $a_{\varepsilon,i}$, $b_{\varepsilon,i,j}$ and κ_i values for individual fictitious gray gases are obtained from Ref. [17]. The radiation source term in the flamelet model is then computed as

$$\dot{q}_r''' = 4\left(\kappa_s + \kappa_g\right)\sigma T^4 . \tag{7}$$

The model provides the local radiant emission fraction, Ψ_r, of the turbulent flame sheet taking two inputs from the LES solver, a non-dimensional prior heat loss ("enthalpy defect"), H_p, and a turbulent micro-scale strain rate, a_0 [1]. The prior heat loss fraction, H_p, can be due to soot and gaseous products radiating in the turbulent flame. Convective losses near cold walls can also result in a prior heat loss. A lookup table of $\Psi_r\left(a_0, H_p\right)$ values is created for individual fuels by parametrizing the flamelet model with a range of a_0 and H_p values.

The LES equations

Soot formation and oxidation are not explicitly modeled in the LES of the turbulent flames. Instead, a local volumetric radiant emission term,

$$\tilde{q}_r''' = \Psi_r\left(a_0, H_p\right)\tilde{\omega}_F'''\,\Delta H_c \ , \tag{8}$$

is included in the sensible enthalpy equation in the LES solver. Here, ΔH_c is the fuel heat of combustion and the local fuel consumption rate, $\tilde{\omega}_F'''$, is obtained from the EDM as described above. The local volumetric emission from the turbulent flame-sheet, $\tilde{q}_r'''$, due to soot and gas-phase species is affected by the local turbulent strain rate, a_0, and the prior heat loss, H_p. As in previous studies [1, 2, 3, 4], prior heat loss is computed from the LES solver as

$$H_p = \left(\tilde{h}_s + \tilde{h}^0 - \tilde{Z}h^0_{F,\infty}\right)\Big/\left(\tilde{h}^0 - \tilde{Z}h^0_{F,\infty}\right), \tag{9}$$

where $\tilde{h}_s$ and $\tilde{h}^0$ are the resolved sensible and chemical enthalpies, respectively, $\tilde{Z}$ is the mixture fraction estimated from the computed species mass fractions and $h^0_{F,\infty}$ is the fuel heat of formation. In presence of a cold wall, the local sensible enthalpy, $\tilde{h}_s$, reduces, resulting in H_p increasing (a value of $H_p > 0$ implies a local enthalpy defect/loss). Local radiant emission from the flame-sheet located at an upstream region also causes the H_p value to increase in the downstream. Consistent with previous studies [1, 2], the turbulent/subgrid micro-scale strain rate is estimated as $a_0 = C_\eta\left(1/\tau_\eta\right)$, where the Kolmogorov time-scale, τ_η, is computed from the viscosity, ν, and the subgrid dissipation rate, ε_{sgs}, as $\tau_\eta = \left(\nu/\varepsilon_{sgs}\right)^{1/2}$, with $C_\eta = 0.04$ [1, 2]. In the present study, an enhancement to the strain rate estimation method is proposed. In order to estimate a strain rate relevant to the soot formation process in regions where the computational mesh can resolve the flow (i.e. the subgrid kinetic energy in these cells tends toward zero, $k_{sgs} \to 0$), the smaller of the subgrid and resolved time-scales is used:

$$a_{0,enh} = C_\eta\left(\min\left(\tau_\eta, \left(\sqrt{2}\left|\tilde{S}\right|\right)^{-1}\right)\right)^{-1}. \tag{10}$$

Here, the resolved time-scale is computed as the inverse of the mesh-resolved strain rate $1/\sqrt{2}\left|\tilde{S}\right|$, where $\left|\tilde{S}\right| = \left(\tilde{S}_{ij}\tilde{S}_{ij}\right)^{1/2}$ and $\tilde{S}_{ij} = \left(\partial\tilde{u}_i/\partial x_j + \partial\tilde{u}_j/\partial x_i\right)/2$ [8]. Regions of very low k_{sgs} exist in the upstream flame region (near the burner) in the presence of walls. In these regions, the resolved strain-rate is greater than the subgrid values, as demonstrated below. The local turbulent strain rate affects the laminar flamelet soot formation rate, e.g., the higher the strain rate (i.e., shorter the flamelet residence time), lower the soot formation rate (see Ref. [1] for details).

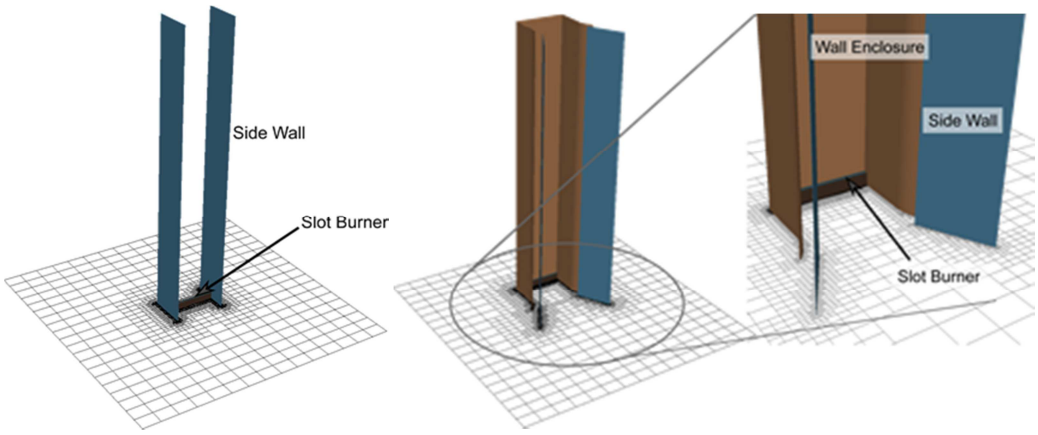

(a) Unconfined (b) Wall-bounded

Fig. 2. Slot burner of length 0.38 m and width 0.016 m (a) with two side walls (unconfined burner setup), and (b) placed adjacent to a wall enclosure of height 2.2 m with slanted side walls (wall-bounded burner setup).

COMPUTATIONAL SETUP

The computational setup shown in Fig. 2(a) consisted of a 0.38 m long by 0.016 m wide slot burner elevated from the ground by 0.05 m (henceforth known as the "unconfined" burner setup). Two walls were placed perpendicular to and attached at the ends of the slot burner to prevent air entrainment from the sides. The slot burner was also placed adjacent to the bottom of a 2.2 m tall and 0.38 m wide wall (henceforth known as the "wall-bounded" burner setup), see Fig. 2(b). The wall enclosure consisted of end walls for ensuring unidirectional air entrainment. In addition, to mimic the experimental setup [7] accurately, two slanted side walls were included in the setup. Gaps were present between the slanted walls and the wall enclosure, as can be observed in Fig. 2(b). The computational mesh comprised primarily of hexahedral cells. A mesh sensitivity analysis was conducted, and a mesh resolution of approximately 0.002 m × 0.002 m × 0.004 m (in the vertical direction) was kept uniform to 0.08 m from the wall all the way up to 2.2 m height. For the unconfined burner simulations, the mesh resolution was kept the same up to a ±0.06 m distance from the burner centerline. The side boundaries were open allowing entrainment of air whereas the ground and walls had non-slip boundary condition applied for velocity. A convective-diffusive inlet boundary condition was applied for the species and velocity at the burner [4]. The temperature of the entrained air from the open boundaries was 298.15 K, the ground temperature was held constant at 298.15 K, whereas the 2.2 m tall wall was kept at 333 K.

RESULTS AND DISCUSSION

Ethylene fires of chemical heat release rates (HRRs) in the range of 20-60 kW (henceforth reported per unit slot burner length as 51-160 kW/m) have been simulated. The predicted results are compared against experimental data from the study of Markstein and de Ris [7]. In the experiments, the wall was cooled with an inlet water temperature of 60°C [7]. The predicted data are time-averaged for 30 s, neglecting the initial transient period of ~10 s.

Flame structure

In the presence of the isothermal wall (maintained at 333 K or 60 °C), the flame radiant emission distribution changes compared to the unconfined case, as shown in Fig. 3 for the 51 kW/m fire. The flame height also increases when the slot burner is placed adjacent to the isothermal wall. In Fig. 3, for the 51 kW/m fire, the instantaneous flame height can be observed to more than double in the case of the wall-bounded scenario. The wall affects the flame height as half the area for entrainment is available compared to the unconfined case and because of the reduction in the entrainment rate due to suppression of the large-scale eddies causing the local volumetric burning rate to decrease [1].

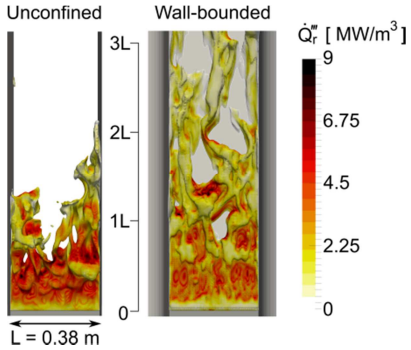

Fig. 3. Instantaneous flame-sheets (iso-contour of stoichiometric mixture fraction colored by volumetric radiant emission) for the 51 kW/m fires: unconfined and attached to the isothermal wall (wall-bounded).

In Fig. 4, time-averaged temperature contours are presented for the 51 and 160 kW/m unconfined and wall-bounded fires. The contours are shown on a plane positioned at the middle of the burner (cross-section view), perpendicular to the lengthwise direction. With increasing HRR, as expected, the peak temperature occurs further downstream for both the unconfined and wall-bounded fires. Near the burner, a laminar to turbulent transition region is visible in the close-up view in Fig. 4(a) of the wall-bounded 51 kW/m fire. In this region, the flames tend to attach to the wall. This region is of much shorter height, as can be observed in the Fig 4(b) close-up view for the 160 kW/m wall-bounded fire.

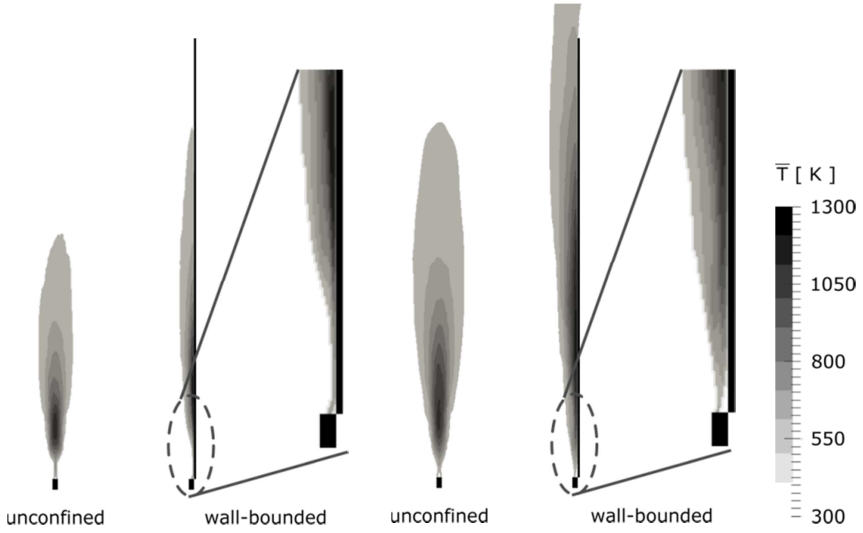

(a) 51 kW/m (b) 160 kW/m

Fig. 4. Time-averaged temperature contours of (a) 51 and (b) 160 kW/m unconfined and wall-bounded fires.

OVERALL RADIANT FRACTION

For the 160 kW/m fire, the predicted radiant fraction reduces from ~0.37 for the unconfined fire to ~0.27 for the wall-bounded fire, a reduction of ~26% compared to an ~32% decline observed in the experiments [7]. The variation of overall radiant fraction as functions of the chemical HRR per unit length of the unconfined and wall-bounded fires is shown in Fig. 5. For the unconfined fires, the radiant fraction is predicted within 6-7% of the experimental values as shown by the solid curve in Fig. 5 (black dashed curve). Using the subgrid micro-scale strain rate estimation, a_0, the overall radiant fractions in the presence of the isothermal wall is found to reduce by 24-26% compared to the predicted values for the unconfined fires (see red dashed curve in Fig. 5). The reduction in overall radiant fractions occur due to the convective losses to the wall causing increase in the prior enthalpy loss fraction, H_p, which results in local reduction in radiant emission from the turbulent flame-sheet. These reductions are smaller compared to the observed trends in the experiments, e.g., for the 51 kW/m fire, a reduction of ~41% in the overall radiant fraction was observed in the experiments.

As can be observed in Fig. 4(a) for the wall-bounded 51 kW/m fire, the flame-sheet tends to attach to the wall very near the slot burner. The flow in this region is transitional and is resolved by the fine mesh used in the simulations. For the larger HRR of 160 kW/m, the transition region is quite short as can be observed in Fig. 4(b). To account for the flow in the transition region, the enhanced

strain rate estimation method was proposed (see numerical model description above). A comparison of the predicted time-averaged strain rates, a_0 and $a_{0,enh}$, is shown in Fig. 6 for the 51 kW/m wall-bounded fire. In Fig. 6(a), the simulation used the subgrid strain rate, a_0, estimated using the Kolmogorov micro-time scale and application of a constant, C_η. It can be observed that unreasonably small strain rates of value $<10^{-1}$ s^{-1}, corresponding to soot-formation residence times of >10 s, are observed near the base of the fire. These subgrid strain rate estimates for application in the subgrid radiation model are found to be incorrect as the turbulent kinetic energy, k_{sgs}, used in the estimate of the turbulent dissipation rate, ε_{sgs}, is almost zero near the base of the fire. Therefore, to more accurately estimate the strain rate for such regions where the flow is resolved by the mesh, a maximum of the strain rate between the subgrid and resolved scales, $a_{0,enh}$, was also applied in additional simulations.

Using the enhanced strain rate formulation, $a_{0,enh}$, the smaller overall radiant fraction values are predicted for the lower HRRs (see blue dashed curve in Fig 5); predicted to be within 7% of the experimental values. This can be attributed to the higher strain rates predicted in the upstream region (near the base of the fire) resulting in shorter flamelet residence times and correspondingly lower soot formation rates. For the 160 kW/m wall-bounded fire though, a <4% change in the predicted overall radiant fraction was observed between the two strain rate estimation methods. This is because, for higher HRR, the laminar to turbulent transition region is shorter and the flow is not mesh-resolved, leading to the subgrid micro-scale strain rate to dominate for the majority of the fire region. Smaller than 1% change in the overall radiant fraction was observed for the unconfined fires when using the enhanced strain rate estimation.

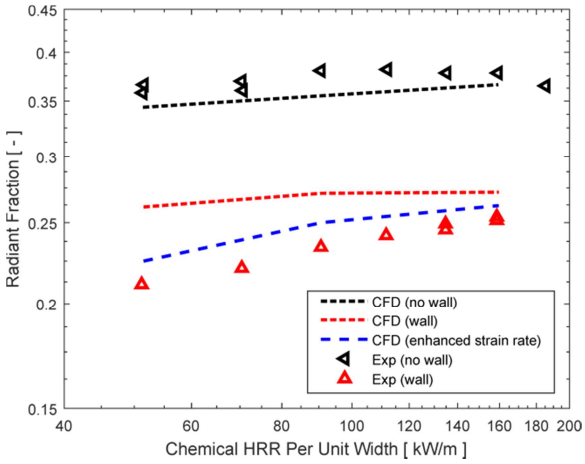

Fig. 5. Computed radiant fractions compared against experimental data.

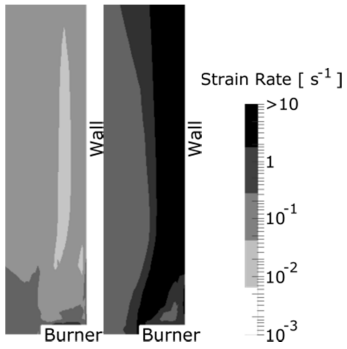

(a) a_0 (b) $a_{0,enh}$

Fig. 6. Time-averaged strain rate contours adjacent to the wall and up to ~0.1 m downstream distance from the burner for the 51 kW/m fire. Strain rate is modeled (a) in the subgrid, a_0, and (b) as a maximum of the subgrid and resolved strain rates, $a_{0,enh}$. A log-scale is used to accentuate the distribution differences.

RADIANT POWER DISTRIBUTIONS

The predicted radiant power distributions as functions of height above the burner, $\dot{q}_r'(z - z_0)$, where $z_0 = 0.05$ m is the burner height, are next compared against experimental data in Fig. 7. For both

the unconfined and wall-bounded fires, the predicted peak radiant power increases with increasing HRR. The height at which peak radiant power occurs is predicted to be closer to the burner compared to the locations of the experimental peaks for the range of HRRs simulated. The predicted peak values are, however, within 10-11% of the experimental values for the unconfined fires. Irrespective of the strain rate estimation method applied, a_0 or $a_{0,enh}$, the radiant power profiles for the unconfined fires are not significantly affected. For the wall-bounded fires, when using the subgrid micro-scale strain rate, a_0, the peak value is over-predicted by ~75% for the 51 kW/m, ~29% for the 91 kW/m and ~5% for the 160 kW/m fires. The increasing difference between the predicted and experimental peak values with decreasing HRRs also manifests itself in the overall radiant fraction over-prediction, as discussed above. The radiant profiles beyond the peaks for the 91 and 160 kW/m fires are seen to follow the experimental slopes though, showing reasonably good match with experimental data.

The reduction in radiant peak power occurs due to the convective heat loss to the adjacent isothermal wall. The peak radiant power shows greater decline with reducing HRR, which can be attributed to the greater convective heat loss to the wall observed for the lower HRR fires as shown in Fig. 8 (the x-axis is normalized by the flame height, ℓ_f, which is the height above the burner where the time-averaged radiant power output is zero). The time-averaged peak convective heat flux to the wall (vertical distribution on the centerline of the isothermal wall) is ~15% higher for the 51 kW/m wall-bounded fire compared to the 160 kW/m fire. The wall-integrated heat flux for the flame region, i.e., for the normalized height, $\left(z-z_0\right)/\ell_f$, from 0 to 1, increases from 4 kW to 7 kW when the HRR increases from 51 to 160 kW/m. The convective loss fraction to the isothermal wall is ~8% for the 51 kW/m, ~6% for the 91 kW/m and ~4% for the 160 kW/m fires. This decrease in the convective loss fraction causes an increase in the overall radiant fraction with increasing HRR for the wall-bounded fires.

Compared to the unconfined fires, the model however predicts lower radiant power output in presence of the isothermal wall. The difference between the unconfined and wall-bounded radiant power is primarily attributed to the convective losses to the isothermal wall as postulated by Markstein and de Ris [7]. However, in the experiments, the overall radiant fraction and the peak radiant power showed a greater reduction with decreasing HRR compared to the model predictions. The reasons for the model over-prediction of radiant power in the presence of the isothermal wall was found to be the use of the subgrid strain rate, a_0, for determination of the local radiant output from the flame-sheet. In regions where the flow is resolved by the computational mesh, the a_0 values are estimated to be unrealistically low, as discussed above.

It was found that for the unconfined fires the difference in predictions was minor when using either of the strain rate estimation methods (a_0 or $a_{0,enh}$). However, the predicted radiant power output for the wall-bounded fires was affected significantly, particularly for the 51 kW/m case, as shown in Fig. 7(a). The peak radiant power was predicted with greater accuracy using the $a_{0,enh}$ strain rate estimation. The peak radiant power locations were predicted to be closer to the experimental values for the 91 and 160 kW/m wall-bounded fires as well, as can be seen in Fig. 7(c-d). Using the enhanced strain rate, $a_{0,enh}$, the peak radiant power locations were also closer to the heights where the experimental peaks were observed. The convective heat loss fraction (i.e. compared to the fire HRR) does not change significantly with the use of the enhanced strain rate, $a_{0,enh}$. This shows that, besides convective losses to the wall, the strain rates in the near-wall region also need to be accurately predicted for better estimation of the radiant power distributions.

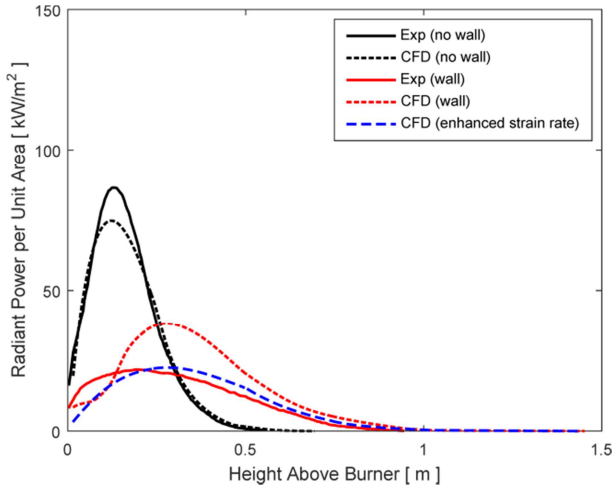

(a) 51 kW/m

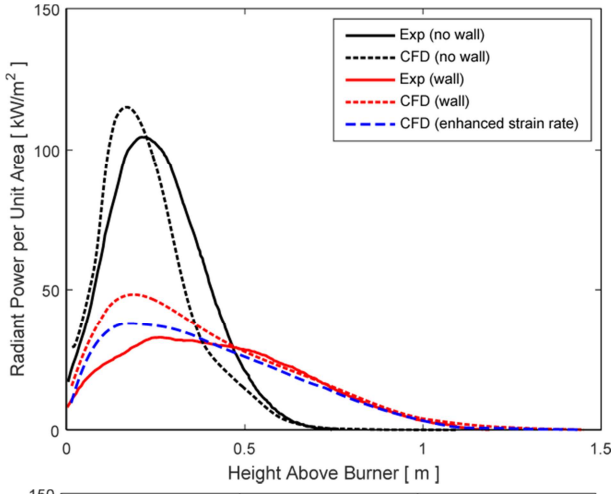

(b) 91 kW/m

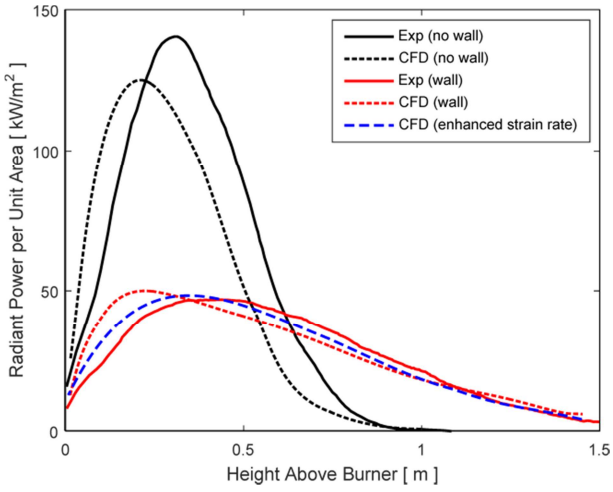

(c) 160 kW/m

Fig. 7. Predicted radiant power per unit area compared against experimental data for (a) 51 kW/m, (b) 91 kW/m and (b) 160 kW/m unconfined and wall-bounded fires.

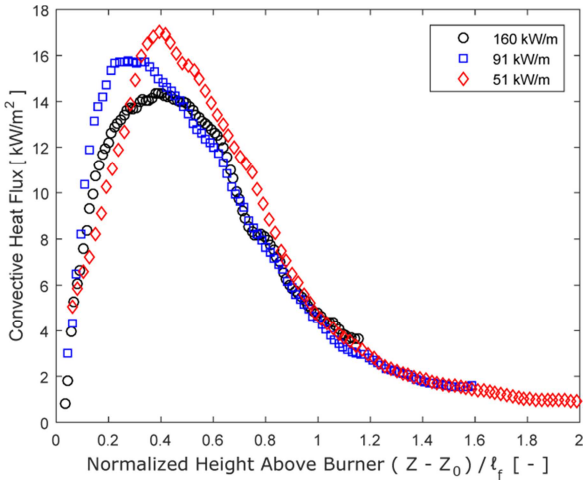

Fig. 8. Time-averaged vertical distributions of convective heat flux on the centerline of the isothermal wall. The height above the burner, $z - z_0$, is normalized by the computed flame heights (ℓ_f).

CONCLUSIONS AND FUTURE WORK

LES of wall-bounded slot burner fires were performed using the FireFOAM code. Radiant power distributions and overall radiant fractions were predicted and compared against experimental data. Predicted overall radiant fraction and peak radiant power output were found to decrease when the unconfined fires were placed adjacent to an isothermal wall due to the convective heat losses to the wall. The reductions to the overall radiant fraction were ~25% irrespective of the HRR when a subgrid strain rate was used as input to the radiation model. When using this strain rate estimation method, as was previously done in studies involving unconfined fires [1, 2], comparison with experimental data showed favorable agreement of radiant power output profiles for the unconfined fires. However, for the wall-bounded fires, it was found that using a maximum between the subgrid micro- and resolved-scale strain rates improved the radiant power and overall radiant fraction predictions, especially for the lower HRR cases. The present study validates the subgrid, flamelet-based radiation model [1, 2] for applications in wall-bounded fire simulations. Predictions showed that the convective losses to the isothermal wall were modeled, resulting in lowering of the overall radiant output from the wall-bounded fires. However, it was found that a more accurate estimation of the strain rate affecting the soot formation process is required for mesh-resolved flow which occurs in the upstream regions of the wall-bounded fires. This is especially true for lower HRR fires which have longer laminar to turbulent transition regions near the burner. The validated radiation model will be applied in the future toward LES of wall-fires with prescribed fuel supply from porous wall burners [1]. Further improvements in the predictions of the convective heat transfer and strain rate need to be made, especially to determine their sensitivity to mesh resolution near the wall.

ACKNOWLEDGEMENTS

The authors wish to thank Dr. Ning Ren for his feedback and thoughtful discussions on wall-bounded fires. The work presented in this paper is funded by FM Global and performed within the framework of the FM Global Strategic Research Program on Fire Modeling.

REFERENCES

[1] P. Chatterjee, J.L. de Ris, Y. Wang, S.B. Dorofeev, A Model for Soot Radiation in Buoyant Diffusion Flames, Proc. Combust. Inst. 33 (2011) 2665–2671.

[2] P. Chatterjee, Y. Wang, K.V. Meredith, S.B. Dorofeev, Application of a Subgrid Soot-Radiation Model in the Numerical Simulation of a Heptane Pool Fire, Proc. Combust. Inst. 35 (2015) 2573–2580.

[3] G.H. Markstein, J. de Ris, Wall-fire Radiant Emission. Part 2: Radiation and Heat Transfer from Porous-metal Wall Burner Flames, Proc. Combust. Inst. 24 (1992) 1747–1752.

[4] FireFOAM: Available from http://www.fmglobal.com/modeling (accessed 6 August 2018).

[5] Y. Wang, P. Chatterjee, J.L. de Ris, Large Eddy Simulations of Fire Plumes, Proc. Combust. Inst. 33 (2011) 2473–2480.

[6] C.W. Lautenberger, J.L. de Ris, N.A. Dembsey, J.R. Barnett, H.R. Baum, A Simplified Model for Soot Formation and Oxidation in CFD Simulation of Non-premixed Hydrocarbon Flames, Fire Saf. J. 40 (2005) 141–176.

[7] G.H. Markstein, J. de Ris, Wall-fire Radiant Emission. Part 1: Slot-burner Flames, Comparison with Jet Flames, Proc. Combust. Inst. 23 (1990) 1685–1692.

[8] OpenFOAM: Available from http://www.openfoam.org (accessed 6 August 2018).

[9] B.F. Magnussen, B.H. Hjertager, On Mathematical Modeling of Turbulent Combustion with Special Emphasis on Soot Formation and Combustion, Proc. Combust. Inst. 16 (1977) 719–729.

[10] C. Fureby, G. Tabor, H.G. Weller, A.D. Gosman, A Comparative Study of Subgrid Scale Models in Homogeneous Isotropic Turbulence, Phys. Fluids 9 (1997) 1416–1429.

[11] S. Krajnović, L. Davidson, A Mixed One-equation Subgrid Model for Large Eddy Simulation, Int. J. Heat Fluid Flow 23 (2002) 413–425.

[12] W. Kim, S. Menon, A New Dynamic One-equation Subgrid-scale Model for Large Eddy Simulation, 33rd Aerospace Sciences Meeting and Exhibit, Reno, NV, 1995.

[13] G.F. Carrier, F.E. Fendell, F.E. Marble, The Effect of Strain Rate on Diffusion Flames, SIAM J. App. Math. 28 (1975) 463–500.

[14] C.L. Tien, K.Y. Lee, A.J. Stretton, Radiation Heat Transfer, in: The SFPE Handbook of Fire Protection Engineering. National Fire Protection Association, Quincy, MA, 3rd ed, 2002.

[15] H.C. Hottel, A.F. Sarofim, Radiative Transfer, McGraw Hill, New York, 1967.

[16] J. de Ris, Fire Radiation – A Review, Proc. Combust. Inst. 17 (1979) 1003–1015.

[17] T.F. Smith, Z.F. Shen, J.N. Friedman, Evaluation of Coefficients for the Weighted Sum of Gray Gases Model, J. Heat Transfer 104 (1982) 602–608.

[18] A. Atreya, S. Agrawal, Effect of Radiative Heat Loss on Diffusion Fames in Quiescent Microgravity Atmosphere, Combust. Flame 115 (1998) 372–382.

[19] S.J. Brookes, J.B. Moss, Predictions of Soot and Thermal Radiation Properties in Confined Turbulent Jet Diffusion Flames, Combust. Flame 116 (1999) 486–503.

[20] M.A. Delichatsios, Flame Heights in Turbulent Wall Fires with Significant Flame Radiation, Combust. Sci. Technol. 39 (1984) 195–214.

[21] N. Ren, Y. Wang, S. Vilfayeau, A. Trouvé, Large Eddy Simulation of Turbulent Wall Fires Supplied with Gaseous Fuel through Porous Burners, Combust. Flame 169 (2016) 194–208.